High-Fidelity Bell-State Preparation with $^{40}Ca^+$ Optical Qubits

Craig R. Clark, Holly N. Tinkey, Brian C. Sawyer, Adam M. Meier, Karl A. Burkhardt, Christopher M. Seck,[†] Christopher M. Shappert, Nicholas D. Guise, Curtis E. Volin,[‡] Spencer D. Fallek, Harley T. Hayden, Wade G. Rellergert, and Kenton R. Brown[*]
Georgia Tech Research Institute, Atlanta, Georgia 30332, USA

(Received 30 June 2021; accepted 19 August 2021; published 24 September 2021)

Entanglement generation in trapped-ion systems has relied thus far on two distinct but related geometric phase gate techniques: Mølmer-Sørensen and light-shift gates. We recently proposed a variant of the light-shift scheme where the qubit levels are separated by an optical frequency [B. C. Sawyer and K. R. Brown, Phys. Rev. A **103**, 022427 (2021)]. Here we report an experimental demonstration of this entangling gate using a pair of $^{40}Ca^+$ ions in a cryogenic surface-electrode ion trap and a commercial, high-power, 532 nm Nd:YAG laser. Generating a Bell state in 35 μs, we directly measure an infidelity of $6(3) \times 10^{-4}$ without subtraction of experimental errors. The 532 nm gate laser wavelength suppresses intrinsic photon scattering error to $\sim 1 \times 10^{-5}$.

DOI: 10.1103/PhysRevLett.127.130505

Generation of 2-qubit entanglement is a key element of universal quantum computing [1] and is typically the most difficult operation to execute with the necessary high fidelity and short duration. The past two decades have seen marked improvement in the measured fidelities for quantum operations across multiple physical qubit platforms, including atomic [2–4], molecular [5], solid-state [6,7], and photonic systems [8]. The highest-fidelity 1- and 2-qubit operations are currently performed using laser-cooled atomic ions confined in three-dimensional radio frequency (rf) Paul traps, where 2-qubit gate fidelities of 0.993 ($^{40}Ca^+$, 50 μs gate duration) [9], 0.999 ($^{43}Ca^+$, 100 μs gate duration) [10], and 0.9992 ($^{9}Be^+$, 30 μs gate duration) [11] have been demonstrated with lasers. Recently a related rf-based operation with a fidelity confidence interval of [0.9983, 1] ($^{25}Mg^+$, 740 μs gate duration) was performed in a surface-electrode ion trap [12]. In Refs. [10–12], the reported 2-qubit gate fidelities are computed from state tomography measurements by correcting for state preparation error and also, in Ref. [10], for 1-qubit operation errors. In this Letter, we report the generation of a 2-qubit Bell state [13] in 35.2 μs with a fidelity of 0.9994(3) as measured via Bell-state tomography without correcting for error sources in postprocessing.

Laser-based entanglement generation in trapped-ion systems has until now relied largely on two distinct but related 2-qubit geometric phase gate techniques: Mølmer-Sørensen (MS) [14] and light-shift (LS) [15] gates. Laser-based entangling gates for qubit levels within the $S_{1/2}$ manifold of atomic ions typically require ultraviolet wavelengths for efficient MS or LS gate operations. Alternatively, optical qubits employing narrow atomic transitions (e.g., $S_{1/2} - D_{5/2}$) allow for visible or infrared laser wavelengths for MS gates [9,16], but with the trade-off that optical phase stability must be maintained throughout the entangling operation.

We have recently proposed a variant of the LS gate scheme where the qubit levels are separated by an optical frequency and the gate laser wavelength is far detuned from any atomic resonance [17]. Some advantages of this optical transition dipole force (OTDF) gate include compatibility with dynamical decoupling pulse sequences [15,18], a broad range of feasible entangling gate laser wavelengths (including visible wavelengths), 2-qubit photon scattering error below 10^{-4} in some wavelength regimes, and straightforward extension to cotrapped disparate species group-2 ions. As in other optical-qubit systems, our gate is sensitive to the optical phase of the laser used for 1-qubit operations; however, the compatibility of $\sigma^z\sigma^z$ gates with dynamical decoupling pulses that suppress phase errors mitigates this effect. We report here an experimental demonstration of the OTDF gate using a cotrapped pair of $^{40}Ca^+$ in a surface-electrode ion trap.

The ions are confined 30 μm above the trap surface in a fixed potential with axial center-of-mass (c.m.) mode frequency $\omega_{\text{c.m.}} = 2\pi \times 2.53$ MHz, breathing-motion (BM) mode frequency $\omega_{\text{BM}} = 2\pi \times 4.38$ MHz, and radial mode frequencies $\sim 2\pi \times 8$ MHz. Confinement transverse to the symmetry axis is achieved via rf potentials applied to the radial electrodes with amplitude $\sim$100 V at 144 MHz. Static (dc) potentials for confinement along the axis are supplied by digital-to-analog converters and are filtered at the vacuum chamber by 2 Hz low-pass filters to suppress electronic noise that can lead to variations in the trap frequency or in the center of the trap potential [19,20]. A magnetic field of 1.07 mT provided via a temperature-stabilized NdFeB permanent magnet outside the vacuum chamber establishes the quantization direction, which is oriented $\sim$45° from the axis as shown in Fig. 1.

The ion trap is installed in an ultrahigh-vacuum cryogenic chamber based on a Gifford-McMahon closed-cycle cooler. Cryogenic operation is not a requirement for the gate but is useful to reduce anomalous heating in some cases [21] and to prolong ion lifetimes via cryopumping [22]. The trap mounting fixture is attached to an optical table below via a series of metal and ceramic stand-offs, which provides a solid mechanical reference to the table surface while maintaining sufficient thermal isolation between room temperature, the intermediate stage, and the cold stage. The trap fixture is anchored thermally to the cold stage via copper braids and reaches a temperature of 8.5 K during application of the rf trapping potential. Interferometric measurements reveal trap-mount vibrations along the trap symmetry axis at the level of 30 nm root mean square, with peak excursions up to 80 nm, and dominated by oscillations at the 1.3 Hz cryocooler cycle frequency.

As in Ref. [17], we choose $|\downarrow\rangle = S_{1/2}(m_j = 1/2)$ and $|\uparrow\rangle = D_{5/2}(m_j = 3/2)$ as the qubit states. This optical-qubit transition frequency is linearly sensitive to magnetic field variations, which thereby form a potentially large source of decoherence in our experiments, but the incorporation of a Hahn spin echo into the OTDF gate mitigates this deficiency [15,23]. We perform 1-qubit rotations with a narrow-linewidth 729 nm Ti:sapphire laser locked to an ultrahigh-finesse cavity. The 729 nm laser beam is used both for the spin echo π pulse and for the $\pi/2$ pulses of Fig. 1(b) employed for Bell-state creation and parity analysis.

We intersect two 532 nm entangling gate beams at an angle of 90° [see Fig. 1(a)] to create a moving optical lattice that drives the ions with a spin-dependent optical-dipole force (ODF). We choose to generate entanglement with a wavelength of 532 nm, where high-power single-longitudinal-mode lasers are readily available and where photon scattering errors are nearly minimized [17]. The wave vector difference between the beams is oriented along the z axis, so that only the motional modes along this direction are driven. Each beam has a waist of approximately 10 μm and linear polarization along y to maximize optical interference.

The detuning $(\omega_{\mathrm{BM}} + \delta)$ between the beams is chosen such that the gate detuning δ is closer to the BM mode than it is to the c.m. This mitigates the impact of mode heating during the gate (the BM mode heats at <1.4 quanta/s compared to 33(14) quanta/s for the c.m.). For appropriate ODF pulse durations and detunings, it is possible to close the paths of both modes in motional phase space. In practice, δ differs from the value $2\pi/\tau_{\mathrm{ODF}}$ that would be chosen for square pulses of duration τ_{ODF}, because we employ a ramped intensity profile (3.2 μs duration) at the beginning and end of the pulses. A power of ~100 mW in each beam achieves the phase gate with two ODF pulses at $\delta \approx 2\pi \times 114$ kHz and $\tau_{\mathrm{ODF}} = 12$ μs.

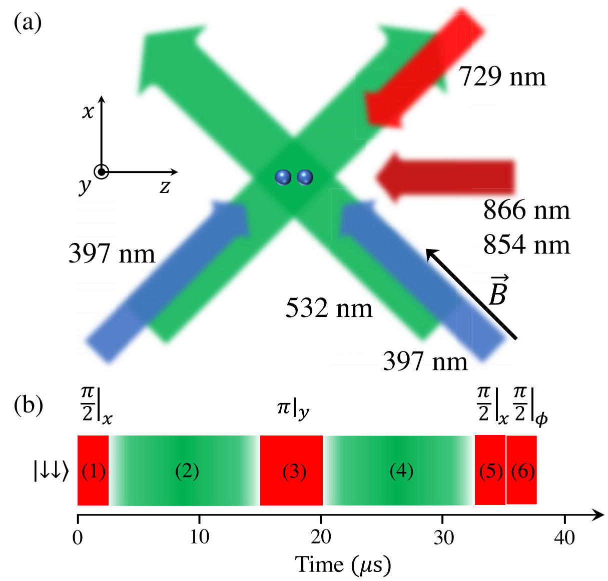

FIG. 1. (a) Illustration of the experimental orientations of laser beams and the bias magnetic field $\vec{B}$ relative to the two-ion $^{40}Ca^+$ crystal. (b) Experimental pulse sequence used in this work for Bell-state generation and parity analysis. Global 1-qubit pulses (1), (3), (5), and (6) are implemented with a resonant 729 nm laser beam. The $\sigma^z\sigma^z$ interactions are produced in pulses (2) and (4) with a pair of 532 nm laser beams intersecting at 90°. The spin-dependent displacements of (2) and (4) are applied with a relative phase offset that minimizes the residual spin-motion entanglement at detuning δ from the axial breathing mode. The Bell state is created in 35.2 μs using pulses (1)–(5).

The ODF beams are created from a single seed laser whose intensity is controlled via an acousto-optic modulator (AOM). Using this AOM, we ramp the intensities of both beams in tandem with sine-squared tapers at the beginning and end of each ODF pulse; such adiabatic ramping is important to suppress sensitivity to the absolute phase of the optical lattice [10,17]. Each of the ODF beams passes in turn through an additional AOM, so that its frequency and phase can be controlled independently and its intensity can be stabilized via monitoring and feedback.

We use the Ramsey sequence depicted in Fig. 1(b) to translate the spin-dependent phase shifts imparted from the ODF interaction into population imbalances that can be determined via optical fluorescence detection. First the ions are Doppler laser cooled with beams at 397 and 866 nm. Then the BM and c.m. modes are cooled below 0.1 quanta via pulsed resolved-sideband cooling on the $S_{1/2}(m_j = -1/2) \rightarrow D_{5/2}(m_j = -5/2)$ transition. The ions are then initialized to $S_{1/2}(m_j = 1/2)$ via a combination of 397 nm excitation with circularly polarized light and seven subsequent iterations of frequency-selective two-step optical pumping through the $D_{5/2}$ and $P_{3/2}$ levels [24]. With the qubits now in the state $|\downarrow\downarrow\rangle$, the experiment follows the Ramsey sequence diagrammed in Fig. 1(b): a first $\pi/2$ pulse (1) creates a superposition of all four 2-qubit states.

The ODF beams are then applied (2) for a duration τ_{ODF} to drive the ions around a closed trajectory in motional phase space, thereby imparting a spin-dependent geometric phase. To symmetrize the phase imparted onto each state within a given parity subspace, the qubits are flipped with a π pulse (3) and subsequently driven with a second ODF pulse (4) nominally identical to the first. However, the ODF phase of (4) is adjusted to match the initial phase of (2) in the rotating frame of the qubit. A second $\pi/2$ pulse (5) then terminates the Ramsey sequence to create the desired Bell state. An optional third $\pi/2$ pulse with variable phase (6) is used for tomographic analysis. Finally, fluorescence at 397 nm is collected from both ions simultaneously for a duration of 100 or 200 μs (see Supplemental Material [24]), and the experiment is repeated to build histograms of detected photon counts.

The resulting photon count histograms are well approximated as a weighted sum of three Poissonian histograms (a two-parameter probability mass function) corresponding to two bright ions ($|\downarrow\downarrow\rangle$), a single bright ion ($|\downarrow\uparrow\rangle$ and $|\uparrow\downarrow\rangle$), and two dark ions ($|\uparrow\uparrow\rangle$). We determine the populations in these three subspaces (P_0, P_1, and P_2, respectively) by maximizing the likelihood of a given observed histogram within this two-parameter model (see Supplemental Material [24]).

To properly suppress errors due to gate detuning fluctuations, it is important that the spacing between the ions be an integer multiple of the lattice wavelength. If this were not the case, the ODF on $|\downarrow\downarrow\rangle$ would not match that on $|\uparrow\uparrow\rangle$, and Walsh modulation would not be achieved via the spin echo [17,18]. For this calibration, we apply an on-resonance ODF pulse ($\delta = 0$) to ions initialized in $|\downarrow\downarrow\rangle$ and look for resulting motion in the BM mode as quantified by excitation of its red motional sideband. We then vary the axial confinement strength and repeat this process so as to minimize the observed excitation. Similarly, the ODF intensity on the two ions should be matched for optimum performance. This is achieved by performing a Ramsey experiment with only a single ODF beam illuminating the ions and maximizing the beat note period observed in the populations as the length of the Ramsey experiment is varied.

For a fixed ODF interaction time, we choose a gate detuning δ to maximize the entanglement fidelity. Figure 2 shows state populations P_0', P_1', and P_2' (the prime notation denotes populations measured before the final analysis pulse) after the second $\pi/2$ pulse (5) as δ is varied; here we intentionally compensate for the change in phase between the two ODF pulses for each δ, so the ODF should have the same phase (in the rotating frame) at the start of each pulse, and P_1' is minimized accordingly for all gate detunings. Experimental data are represented as points with error bars, and the solid lines are theoretical predictions with a 2 kHz offset in detuning as a free parameter. The optimum gate detuning lies near $\delta = 2\pi \times 114$ kHz, where P_0' and P_2' are measured with equal probability. For gate calibration, we use an analytic estimate of the ideal detuning based on the chosen pulse durations and shapes; then we sweep the intensity of the ODF beams to ensure that the even-parity populations are matched for this choice of δ.

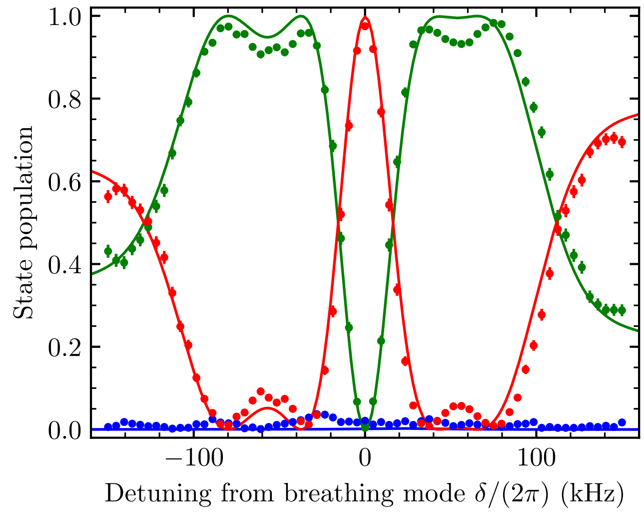

FIG. 2. Measured (points with error bars) and simulated (solid lines) two-ion populations for varying optical-dipole-force detuning δ from the axial breathing motional mode. We measure the two-ion bright (green, P_0'), two-ion dark (red, P_2'), and one-ion bright (blue, P_1') populations at each detuning value (error bars represent the 68% confidence interval assuming binomial statistics). The simulated populations are obtained via numerical integration of the Schrödinger equation, including non-Lamb-Dicke effects.

Figures 3 and 4 show the results of performing this experiment for varying values of the analysis pulse (6)

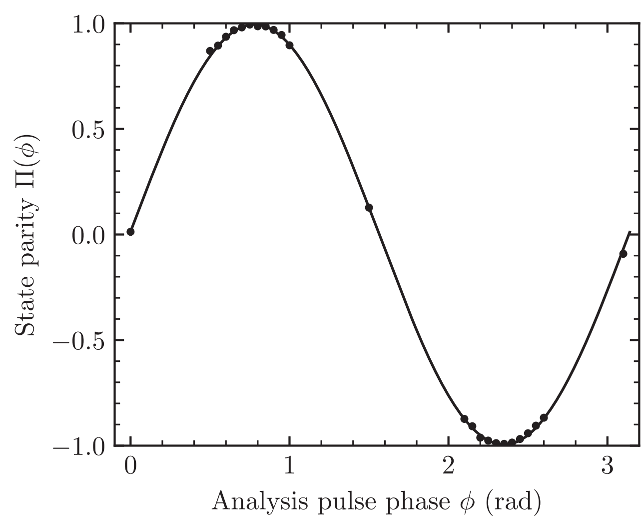

FIG. 3. Two-ion parity measurements (points with error bars) and sinusoidal fit (solid line) versus analysis phase (error bars represent the 68% confidence interval assuming binomial statistics). The density of measured points is highest near the peaks of the parity oscillation. In some cases, the error bar is smaller than the plot marker.

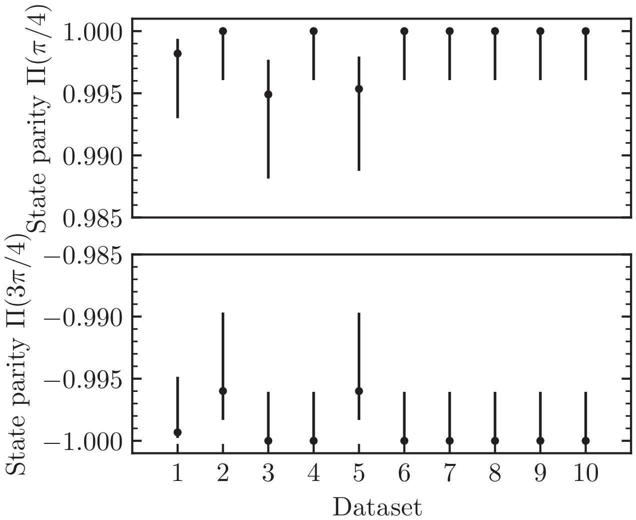

FIG. 4. Repeated measurements of the two-ion parity for alternating values of analysis phase corresponding to the peak amplitudes of Fig. 3 (error bars represent the 68% confidence interval assuming binomial statistics).

phase ϕ. Figure 3 gives the parity $\Pi(\phi) = P_0 + P_2 - P_1 = 1–2P_1$ of the observed final state as a function of ϕ, revealing the expected periodicity of π for a two-spin Bell state. The parity very nearly approaches 1 near $\phi = \pi/4$ and -1 near $\phi = 3\pi/4$. To measure the maximum and minimum values of this curve more efficiently, the experiment was repeated 10 000 times, alternating for each repetition between these two discrete phase values. To look for possible time dependence in the experiments, we binned the results into ten datasets each with 2×500 repetitions and determined the parity of each dataset (Fig. 4). Here we use a Jeffrey's interval to estimate the error bars for each point [26], because the datasets are too small for resampling to yield a meaningful error bar. Six of the datasets are consistent with unity parity amplitude, while four exhibit a small reduction.

To establish the most precise value of the parity amplitude from these data, we determine the parity of all 5000 repetitions at $\phi = \pi/4$ (0.999 02) and at $\phi = 3\pi/4$ ($-0.999\,20$), yielding a parity amplitude of $A = 0.999\,11$. To estimate the uncertainty of this value, we perform bootstrap resampling as follows. Each experiment gives a measured number of photon counts. All of the counts for $\phi = \pi/4$ are binned into a single dataset with 5000 results, and all of the counts for $\phi = 3\pi/4$ are binned into another dataset. We then generate 10 000 bootstrap datasets by resampling from the experimental datasets with replacement, and we analyze each such bootstrapped dataset as described above. The mean of the resulting distribution is 0.999 10 with a 68% confidence interval of $[0.998\,53, 0.999\,61]$, showing that the resampling is not biased significantly.

Similar experiments without an analysis pulse (6) are also performed. Here we repeat the experiment 10 000 times, bin the results into ten datasets each with 1000 repetitions, and determine the residual odd-parity population P'_1 in each dataset (Fig. 5). Seven of the datasets are consistent with $P'_1 = 0$, while three exhibit a small deviation. Treating all 10 000 repetitions as a single dataset yields $P'_0 + P'_2 = 1 - P'_1 = 0.99977$. Resampling as before from this dataset to create 10 000 bootstraps gives a distribution with a mean of 0.999 76 and a 68% confidence interval of $[0.999\,56, 1.000\,00]$, again showing that the distribution is not biased.

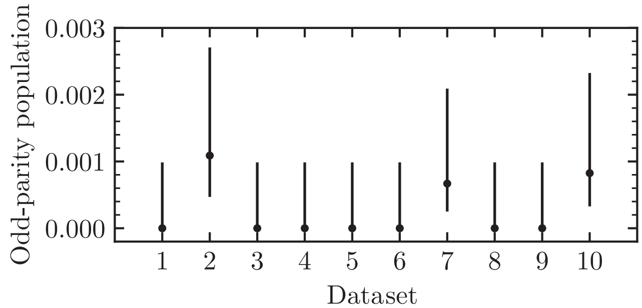

FIG. 5. Repeated measurements of the one-ion bright population P'_1 before a parity analysis pulse (error bars represent the 68% confidence interval assuming binomial statistics).

From these measurements we can obtain an estimate of the Bell-state fidelity F via the relation $F = \frac{1}{2}(P'_0 + P'_2 + A) = 0.99944$ [15]. Using the same 10 000 resampled datasets that were already generated to estimate the parity amplitude A and the populations $P'_0 + P'_2$, we generate a distribution of bootstrapped fidelities (see Supplemental Material [24]). The mean of this distribution is 0.999 43 with a 68% confidence interval of $[0.999\,13, 0.999\,73]$, corresponding to an infidelity of $6(3) \times 10^{-4}$.

Estimated dominant contributions to the infidelity are summarized in Table I. The first line in the table is an upper bound defined as the difference between our measured Bell-state infidelity and the sum of all separately quantified errors. We report this value here as an upper bound on spin dephasing (i.e., phase and intensity instability of the 729 nm laser beam, intensity instability of the 532 nm laser beams, and fast ambient magnetic field noise). The largest contribution is error from the four 1-qubit rotation pulses (1),

TABLE I. Estimated dominant contributions to Bell-state infidelity. The total error due to spin dephasing is bounded by the difference between the measured Bell-state infidelity and the sum of all other known errors.

Error source	Contribution ($\times 10^{-4}$)
Spin dephasing	<4.1
Metastable $D_{5/2}$ decay	0.6
Detection $D_{5/2}$ decay	0.9
Finite axial mode temperature	0.2
Spontaneous photon scattering	0.1
BM mode heating	0.07
Trap frequency variation	0.01

(3), (5), and (6). Randomized benchmarking measurements of our 1-qubit operations shortly after the Bell-state experiments reveal an error per gate of 1×10^{-4}, so that a naive summation of the errors on our two qubits from these four pulses gives a value of 8×10^{-4}. This is clearly an overestimate of their impact on our entangling gate experiments, but is the same order of magnitude as the upper bound of Table I. A more detailed discussion of the various error sources is found in the Supplemental Material [24].

In conclusion, we have demonstrated an OTDF entangling gate using a pair of $^{40}Ca^{+}$ ions in a surface-electrode ion trap, measuring a Bell-state fidelity of 0.9994(3) via parity analysis. Of the estimated experimental error sources, global 1-qubit operations constitute the largest single error by roughly one order of magnitude. By contrast, intrinsic sources of decoherence (spontaneous photon scattering at 532 nm and metastable D-state decay) impart a combined error of $\sim 7 \times 10^{-5}$. Future improvements in the frequency stability of the 729 nm laser system toward the state of the art [27] should significantly increase our Bell-state fidelity. Straightforward extension of the OTDF technique to multispecies ion crystals is detailed in Ref. [17], and implementation of this scheme using radial modes would allow entanglement generation within longer ion chains. Operation at longer (i.e., infrared) wavelengths is also an interesting avenue for further exploration.

This work was done in collaboration with Los Alamos National Laboratory.

[*]Corresponding author.
kenton.brown@gtri.gatech.edu
[†]Present address: Oak Ridge National Laboratory, 1 Bethel Valley Road, Oak Ridge, TN 37830.
[‡]Present address: Honeywell Quantum Solutions, 303 S Technology Ct, Broomfield, CO 80021.

[1] D. P. DiVincenzo, Phys. Rev. A **51**, 1015 (1995).
[2] C. D. Bruzewicz, J. Chiaverini, R. McConnell, and J. M. Sage, Appl. Phys. Rev. **6**, 021314 (2019).
[3] L. Henriet, L. Beguin, A. Signoles, T. Lahaye, A. Browaeys, G.-O. Reymond, and C. Jurczak, Quantum **4**, 327 (2020).
[4] M. Saffman, Natl. Sci. Rev. **6**, 24 (2018).
[5] Y. Lin, D. R. Leibrandt, D. Leibfried, and C.-w. Chou, Nature (London) **581**, 273 (2020).
[6] A. Chatterjee, P. Stevenson, S. De Franceschi, A. Morello, N. P. de Leon, and F. Kuemmeth, Nat. Rev. Phys. **3**, 157 (2021).
[7] M. Kjaergaard, M. E. Schwartz, J. Braumüller, P. Krantz, J. I.-J. Wang, S. Gustavsson, and W. D. Oliver, Annu. Rev. Condens. Matter Phys. **11**, 369 (2020).
[8] J. M. Arrazola *et al.*, Nature (London) **591**, 54 (2021).
[9] J. Benhelm, G. Kirchmair, C. F. Roos, and R. Blatt, Nat. Phys. **4**, 463 (2008).
[10] C. J. Ballance, T. P. Harty, N. M. Linke, M. A. Sepiol, and D. M. Lucas, Phys. Rev. Lett. **117**, 060504 (2016).
[11] J. P. Gaebler, T. R. Tan, Y. Lin, Y. Wan, R. Bowler, A. C. Keith, S. Glancy, K. Coakley, E. Knill, D. Leibfried, and D. J. Wineland, Phys. Rev. Lett. **117**, 060505 (2016).
[12] R. Srinivas, S. C. Burd, H. M. Knaack, R. T. Sutherland, A. Kwiatkowski, S. Glancy, E. Knill, D. J. Wineland, D. Leibfried, A. C. Wilson, D. T. C. Allcock, and D. H. Slichter, Nature (London) **597**, 209 (2021).
[13] M. Nielsen and I. Chuang, *Quantum Computation and Quantum Information: 10th Anniversary Edition*, 10th ed. (Cambridge University Press, Cambridge, 2010).
[14] A. Sørensen and K. Mølmer, Phys. Rev. A **62**, 022311 (2000).
[15] D. Leibfried, B. DeMarco, V. Meyer, D. Lucas, M. Barrett, J. Britton, W. M. Itano, B. Jelenkovic, C. Langer, T. Rosenband, and D. J. Wineland, Nature (London) **422**, 412 (2003).
[16] N. Akerman, N. Navon, S. Kotler, Y. Glickman, and R. Ozeri, New J. Phys. **17**, 113060 (2015).
[17] B. C. Sawyer and K. R. Brown, Phys. Rev. A **103**, 022427 (2021).
[18] D. Hayes, S. M. Clark, S. Debnath, D. Hucul, I. V. Inlek, K. W. Lee, Q. Quraishi, and C. Monroe, Phys. Rev. Lett. **109**, 020503 (2012).
[19] J. M. Pino, J. M. Dreiling, C. Figgatt, J. P. Gaebler, S. A. Moses, M. S. Allman, C. H. Baldwin, M. Foss-Feig, D. Hayes, K. Mayer, C. Ryan-Anderson, and B. Neyenhuis, Nature (London) **592**, 209 (2021).
[20] K. C. McCormick, J. Keller, S. C. Burd, D. J. Wineland, A. C. Wilson, and D. Leibfried, Nature (London) **572**, 86 (2019).
[21] J. Labaziewicz, Y. Ge, P. Antohi, D. Leibrandt, K. R. Brown, and I. L. Chuang, Phys. Rev. Lett. **100**, 013001 (2008).
[22] M. Diederich, H. Häffner, N. Hermanspahn, M. Immel, H. Kluge, R. Ley, R. Mann, W. Quint, S. Stahl, and G. Werth, Hyperfine Interact. **115**, 185 (1998).
[23] E. L. Hahn, Phys. Rev. **80**, 580 (1950).
[24] See Supplemental Material at http://link.aps.org/supplemental/10.1103/PhysRevLett.127.130505 for a discussion of how we extract state populations from fluorescence histograms, for the distribution of bootstrapped fidelities, and for a detailed discussion of gate errors, which includes Ref. [25].
[25] X. R. Nie, C. F. Roos, and D. F. V. James, Phys. Lett. A **373**, 422 (2009).
[26] L. D. Brown, T. T. Cai, and A. DasGupta, Stat. Sci. **16**, 101 (2001).
[27] A. Bermudez, X. Xu, R. Nigmatullin, J. O'Gorman, V. Negnevitsky, P. Schindler, T. Monz, U. G. Poschinger, C. Hempel, J. Home, F. Schmidt-Kaler, M. Biercuk, R. Blatt, S. Benjamin, and M. Müller, Phys. Rev. X **7**, 041061 (2017).